



Parameterization of atmospheric longwave emissivity in a mountainous site for all sky conditions

J. Herrero¹ and M. J. Polo²

¹Fluvial Dynamics and Hydrology Research Group, Interuniversity Research Institute of the Earth System in Andalucía, University of Granada, Spain

²Fluvial Dynamics and Hydrology Research Group, Interuniversity Research Institute of the Earth System in Andalucía, Campus de Excelencia Internacional Agroalimentario ceiA3, University of Cordoba, Spain

Correspondence to: J. Herrero (herrero@ugr.es)

Received: 14 February 2012 – Published in Hydrol. Earth Syst. Sci. Discuss.: 21 March 2012

Revised: 24 July 2012 – Accepted: 20 August 2012 – Published: 5 September 2012

Abstract. Longwave radiation is an important component of the energy balance of the Earth's surface. The downward component, emitted by the clouds and aerosols in the atmosphere, is rarely measured, and is still not well understood. In mountainous areas, direct observations are even scarcer and the fitting of existing models is often subjected to local parameterization in order to surpass the particular physics of the atmospheric profiles. The influence of clouds makes it even harder to estimate for all sky conditions. This work presents a long-time continuous dataset of high-resolution longwave radiation measured in a weather station at a height of 2500 m a.s.l. in Sierra Nevada, Spain, together with the parameterization of the apparent atmospheric emissivity for clear and cloudy skies resulting from three different schemes. We evaluate the schemes of Brutsaert, and Crawford and Duchon with locally adjusted coefficients and compare them with a completely parametric expression adjusted for these data that takes into account three possible significant atmospheric states related to the cloud cover: clear, completely covered, and partly covered skies. All the parametric expressions are related to the screen-level values of temperature, relative humidity and solar radiation, which can be frequently found in standard weather stations. Unobserved cloudiness measurements needed for Brutsaert scheme for cloudy sky are also parameterized from screen-level measurements. The calibration performed for a 6-yr period at the study site resulted in satisfactory estimations of emissivity for all the analyzed schemes thanks to the local fitting of the parameterizations, with the best achievement found for the completely parametric expression. Further validation of the

expressions in two alternative sites showed that the greater accuracy of the latter can also be found in very close sites, while a better performance of the Brutsaert scheme, with a more physical background and the successful parameterization of the clouds effect, is found in nearby sites outside the initial mountain range. The results show the feasibility for the local calibration of expressions to estimate instantaneous atmospheric emissivity for all sky conditions only using surface data, either with a completely parametric scheme if longwave data are available, or through obtaining of locally fitted coefficients for Brutsaert and derived schemes. Nevertheless, the best performance of the first approach would be at the expense of a reduced local applicability.

1 Introduction

Longwave radiation has an outstanding role in most of the environmental processes that take place near the Earth's surface (e.g. Philipona, 2004). Radiation exchanges at wavelengths longer than 4 μm between the Earth and the atmosphere above are due to the thermal emissivity of the surface and atmospheric objects, typically clouds, water vapour and carbon dioxide. This component of the radiation balance is responsible for the cooling of the Earth's surface, as it closely equals the shortwave radiation absorbed from the Sun. The modelling of the energy balance, and, hence, of the longwave radiation balance at the surface, is necessary for many different meteorological and hydrological problems, e.g. forecast of frost and fog, estimation of heat budget from the sea (Dera,

1992), simulation of evaporation from soil and canopy, or simulation of the ice and snow cover melt (Armstrong and Brun, 2008).

Even though longwave radiation instrumentation (pyrgeometer) is nowadays usually deployed at weather stations specifically designed for scientific purposes (e.g. Sicart et al., 2006), it is not so common in the most habitual automated weather stations. Hence, all energy balance models estimate longwave components independently through different physical relations and parameterizations. Downward longwave radiation is difficult to calculate with analytical methods as they require detailed measurements of the atmospheric profiles of temperature, humidity, pressure, and the radiative properties of atmospheric constituents (Alados et al., 1986; Lhomme et al., 2007). To overcome this problem, atmospheric emissivity and temperature profile are usually parameterized from screen-level values of meteorological variables. The use of near surface-level data is justified since most incoming longwave radiation comes from the lowest layers of the atmosphere (Ohmura, 2001).

It is relatively easy to create parameterizations to estimate emissivity under clear sky conditions. Several studies have compared the performance of different parameterizations over longwave records (e.g. Sugitia and Brutsaert, 1993; Gabathuler et al., 2001) and for all cloudy sky conditions (Plüss and Ohmura, 1997; Crawford and Duchon, 1999; Pirazzini et al., 2000; Kjaersgaard et al., 20007; Sedlar and Hock, 2009; Staiger and Matzarakis, 2010). But only a few of them were carried out on highland sites (Iziomon et al., 2003; Lhomme et al., 2007; Flerchinger et al., 2009; Yang et al., 2010). Besides, the effect of clouds and stratification on atmospheric emissivity is highly dependent on regional factors, which may lead to the need for local expressions (e.g. Alados et al., 1986; Barbaro et al., 2010).

But mountainous catchments are very sensitive areas as they are greatly exposed to meteorological conditions. Here, the surface energy balance has the greatest influence on environmental processes, especially if snow is present. As existing measurements are scarce (e.g. Iziomon et al., 2003; Sicart et al., 2006), a correct parameterization of downward longwave irradiance under all sky conditions is essential for these areas. Herrero et al. (2009) modelled the energy balance of the snowpack in Sierra Nevada Mountains (Spain), by the Mediterranean Sea. Different parameterizations for atmospheric longwave emissivity (Brunt, 1932; König-Langlo and Augstein, 1994; Prata, 1996) were tested for clear sky periods, and, although the best model performance was obtained using Brutsaert (1975) (same as Kimball et al., 1982; Kustas et al., 1994; Iziomon et al., 2003), the extension to cloudy conditions (e.g. with Crawford and Duchon, 1999) turned into a global underestimation of incoming longwave radiation. This underestimation prevented the model from reproducing the different winter snow melting cycles typical of this Mediterranean low-latitude area. This problem was overcome through the use of a simple parameterization for

atmospheric emissivity based on 2-yr screen-level values of solar radiation, temperature and relative humidity that greatly improved the simulation of the snow cover evolution (Herrero et al., 2009).

In this work, a deeper analysis of apparent atmospheric emissivity through a 6-yr continuous dataset of measurements of longwave incoming radiation and its relation to other meteorological data in the high mountain site of *Refugio Poqueira* (Sierra Nevada, Spain) is presented. From this analysis, local parameterizations for emissivity under all sky conditions, based on 5-min surface measurements of relative humidity, temperature, and solar radiation, are proposed and validated against direct local measurements. For this purpose, two different approaches were performed and validated at the study site: (1) a new completely empirical expression (3sParam) furthering the results in Herrero et al. (2009); (2) the use of the physically based parameterizations of Brutsaert (1982) (B82) and Crawford and Duchon (1999) (CD99) with a local fitting of their coefficients. Next, the local parameterizations obtained were tested against the data at two additional weather stations: a new station very close to *Refugio Poqueira* with a very similar topography and another station recently deployed on the opposite side of the valley where different orographic conditioning, aspect and elevation can be found. Finally, conclusions concerning the applicability of the different parameterizations developed out of their local scope were addressed.

2 Site description and instrumentation

The study site is the southern slope of Sierra Nevada Mountain (Fig. 1), located 35 km north from the Mediterranean Sea in southeastern Spain (37.5° N). This mountain range rises to 3500 m a.s.l. and runs parallel to the sea for approximately 60 km. It is characterized by high altitudinal gradients and a heterogeneity produced by a high mountain climate influenced by the surrounding Mediterranean climate. The presence and influence of winter snow becomes important at above 2000 m a.s.l. The snowmelt season generally extends from April to June, even though the mild winter periods characteristic of the Mediterranean climate can melt most of the snow before the end of the snow season (especially during January and February). Typically, several consecutive accumulation/melting cycles take place during one year. Sublimation from the snow can also be very important, up to 40 % of yearly snow precipitation, if the appropriate meteorological conditions prevail (Herrero et al., 2009). Sierra Nevada houses a Spanish National Park and one of the International Global Change Observatories in Mountain Areas because of its particular conditions and fragile environment.

An automatic weather station was operated in *Refugio Poqueira* (RP Station), at 2500 m a.s.l. (Herrero et al., 2011). Measurements of incoming shortwave and longwave radiation (Kipp&Zonen SP-Lite pyranometer and CGR3

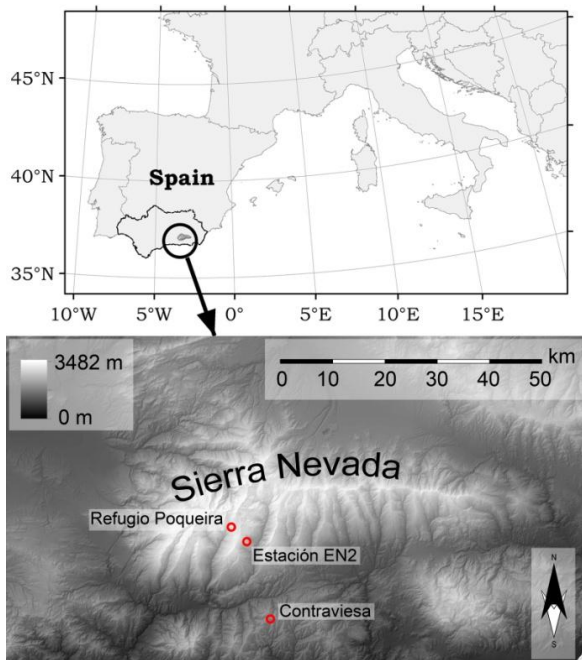


Fig. 1. Location of Sierra Nevada in Andalusia, Spain, and the weather stations used in this study (*Refugio Poqueira* and EN2 on the southern slope of Sierra Nevada; *Contraviesa* facing north on the opposite mountain range).

pyrgeometer) and of 2-m air temperature and relative humidity (Vaisala HMP45), among others, have been conducted continuously since November 2005. The CGR3 pyrgeometer has a spectral range comprised between 4.5 and 44 μm and an accuracy of 5 W m^{-2} . A Campbell CR-510 datalogger recorded 5-min averages of 5 s sampling rate observations. The sensor is placed on a horizontal surface in the middle of the mountain side, surrounded by higher ground to the north but completely exposed to the south. The obstruction of the sky by the terrain is minimal (the sky view factor is 0.97); hence, longwave radiation emitted from the ground has been discarded. Additionally, for this study we have used the data recorded by two new weather stations installed in the proximity of RP Station in 2009 (Fig. 1) that are equipped with downward longwave sensors. (1) EN2 Station, belonging to the Department of Agriculture, Fisheries and Environment of the Regional Government of Andalusia, is located at only 4 km east from RP Station and at 2325 m a.s.l., within the same southern slope of Sierra Nevada. Radiation is measured by a NR01 Hukseflux 4-component net radiometer, while temperature and relative humidity are measured by a Vaisala HMP45. Data are recorded at 10-min intervals. (2) *Contraviesa* Station (C Station) is located at 25 km south from RP Station at 1332 m a.s.l., on the ridge of *Contraviesa* mountain range, which is a lower range parallel to Sierra Nevada. It has the same configuration as RP Station, except for the radiation sensors, which, in this case, are an IR02 pyrgeometer and a LP02 pyranometer, both from Hukseflux.

3 Data analysis

3.1 Longwave data

After the Stefan-Boltzmann Law for the radiation emission of any body at a temperature T (K), downward longwave radiation L^\downarrow (W m^{-2}) coming from the near-surface layer of the atmosphere may be written as

$$L^\downarrow = \varepsilon_a \sigma T_a^4 \quad (1)$$

where ε_a is the apparent emissivity of the sky (Unsworth and Monteith, 1975), σ ($\text{W m}^{-2} \text{K}^{-4}$) is the Stefan-Boltzmann constant, and T_a (K) is the air temperature near the surface (typically 2 m).

The downward longwave radiation measured for 5 consecutive years at RP Station, converted to ε_a according to Eq. (1), is shown in Fig. 2a and summarized in the probability density function (pdf) in Fig. 3. The lower values of ε_a belong to clear sky situations, and in the pdf they smoothly fit a Gaussian with a mean value of 0.68 and a standard deviation of 0.0565. During very clear days, with a low temperature and relative humidity, it exhibits values ranging from 0.5 to 0.6. In the pdf, 0.77 sets the limit between clear sky and partly covered situations; higher values of ε_a denote the presence of clouds in the atmosphere. A seasonal pattern is easily observed in Fig. 2a, where the lowest emissivity values from clear skies are reached during winter. Yang et al. (2010) reported seasonal variations of up to 100 W m^{-2} between summer and winter monthly means of downward longwave radiation measured at the Tibetan Plateau, above 4000 m a.s.l. This emphasizes the importance of longwave balance for cooling the soil and snow under high mountain clear skies. These measurements are similar to those found by Frigero (2004) in Argentina, at 2300 m a.s.l., with night values of atmospheric emissivity of under 0.7 with clear skies. Figure 2b represents daily variation of ε_a , that is, the difference between maximum and minimum daily values. It exhibits a marked seasonality, where wider daily variations of ε_a in winter are in accordance with wider variations in temperature and relative humidity. Minimum instantaneous values of ε_a during winter can be as low as 0.4, while in summer they rarely drop to under 0.6.

These measured values under clear skies are lower than those estimated from the usual empirical expressions, which casts a doubt over the latter for their general use in the highland under any atmospheric state. Thus, the expression by König-Langlo and Augstein (1994), used by Jordan et al. (1999) in the SNThERM model, gives a minimum value for emissivity of 0.765, much higher than the real values measured in this site. Prata (1996) also overestimates the lower values found under clear skies. Only Brutsaert (1975) gives more realistic values of ε_a for clear skies and is capable of reproducing values of below 0.60 during cold days with a clear sky and low relative humidity.

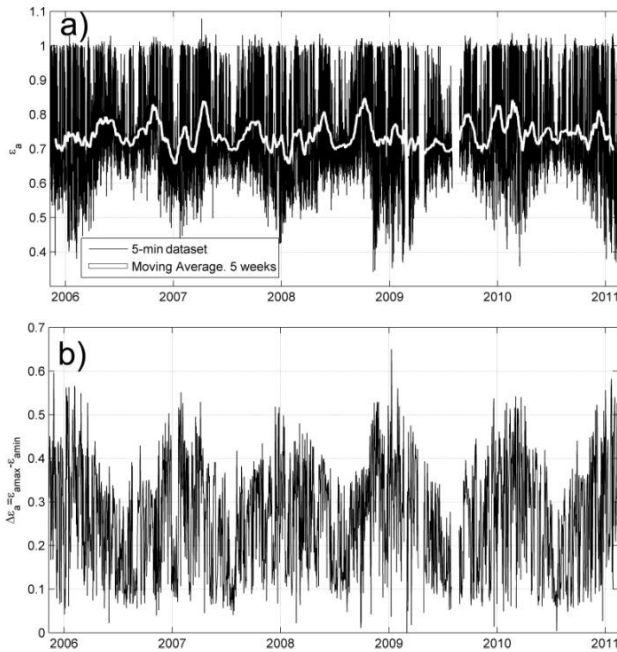


Fig. 2. Atmospheric emissivity measured at RP Station from 2005 to 2011. (a) Complete dataset with 5-min frequency and the 5-week moving average in white. (b) Daily variation (difference between maximum and minimum daily values).

On the other hand, emissivity values of 1 are easily reached under cloudy conditions. The existing parameterizations are required to accomplish this sensitivity to cloud presence, which will usually demand local fitting of the parameters that control the influence of the clouds over emissivity.

3.2 Parameterizations from screen-level data

From the previous analysis of the data recorded by RP Station, it was found that relative humidity, W_a , exhibited more compact relations with ϵ_a and T_a than the water vapour pressure, e_a . So, despite e_a being the variable commonly used in the calculation of ϵ_a for clear skies, W_a was chosen for the parameterizations that involve cloudiness (same as Sicart et al., 2010) because it seems to represent the variation in ϵ_a better, due to the presence of water in the atmosphere at high altitudes. Figure 4a shows the relationship between the measured values of ϵ_a , T_a , and W_a for all sky conditions. That relationship is especially strong for clear and completely covered skies, as shown by the low magnitudes of the standard deviation (std) in Fig. 4b for the values of ϵ_a under 0.7 and over 0.9, respectively. Partly covered skies appear as a transition zone between these two boundary situations. There are some differences in these relationships between daytime and nighttime values, but they were not found to be significant for these particular data.

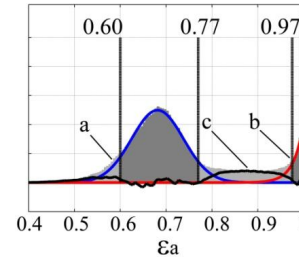


Fig. 3. Pdf of the atmospheric emissivity 5-min values from 2005 to 2011 with (a), a Gaussian fit for clear sky conditions, (b), an exponential fit for completely covered data, and (c) a residual corresponding to partly covered sky situations.

3.2.1 Local 3-state parameterization (3sParam) for RP Station

With a calibration dataset composed of all the 5-min data measured from November 2004 to December 2010 at RP Station, including daytime records for any cloudiness degree, a set of parametric expressions to calculate atmospheric emissivity for all sky conditions was fitted.

In order to evaluate the relationship existing between ϵ_a and cloudiness, the clearness index (CI) has been used, as in Sugita and Brutsaert (1993), and equivalent to ratio s in Crawford and Duchon (1999). CI is the ratio between the theoretical shortwave irradiance at the top of the atmosphere (extraterrestrial radiation) and the surface-measured solar radiation. By means of the CI, calculated with the topographical model described in Aguilar et al. (2010), it is possible to find out the degree of opacity of the atmosphere due to the concentration of aerosols and clouds during the daytime.

Both Figs. 4 and 5 are an image representation of a 3-D surface (T_a - ϵ_a - W_a for Fig. 4, and W_a -CI- ϵ_a for Fig. 5) made up from a cloud of points, which sum up more than 550 000 points corresponding to that number of 5-min measurements at RP Station. In order to visualize them, a grid of 100×100 cells in X-Y axes (T_a - ϵ_a in Fig. 4 and W_a -CI in Fig. 5) was defined and then the mean and the standard deviation of the Z-value (W_a in Fig. 4 and ϵ_a in Fig. 5) of the points included in each cell were calculated and represented through the colour scale. Thus, the image consists of 100×100 cells between the maximum and minimum value in X and Y, and each cell is assigned a colour that corresponds to the mean value or the std in Z of the pixels inside that cell. Cells have to comprise a minimum of 40 points in order to be coloured. Lower values in std refer to that combination of X-Y where Z is very likely to have one particular value, with a low scattering. It is interesting to note that such is the case found for clear skies and for completely covered skies, a property that is used to define different regions for the atmospheric states. The same Fig. 5 shows the states of clear sky (region A) and sky completely overcast (region B) and how they are very well represented in the relation W_a -CI- ϵ_a . The transition area between both

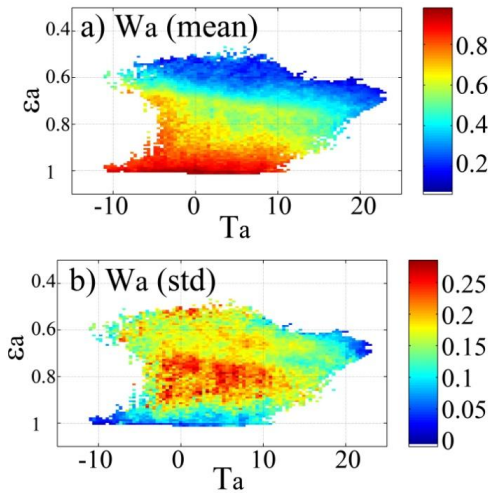


Fig. 4. (a) Mean value and (b) standard deviation for relative humidity W_a measurements as a function of temperature T_a and atmospheric emissivity ϵ_a .

regions concentrates the dispersion of the values (a high std). The region of the completely covered skies has a very high emissivity, of above 0.95. This means that not only are there clouds but also that they are close to the surface, which is common in mountainous areas and the reason why the relative humidity of air is highly correlated with cloudiness.

Thus, a clear sky region (A in Fig. 5a) and a completely overcast region (B in Fig. 5b) were identified from the analyses of the mean values (Fig. 5a) and their std (Fig. 5b). These regions were delimited by the following expressions as a function of W_a and CI:

$$\text{Region A : } CI > 0.25W_a^2 + 0.025W_a + 0.65 \quad (2a)$$

$$CI < -0.25W_a^2 - 0.625W_a + 1.49 \quad (2b)$$

$$\text{Region B : } CI < 2.667W_a - 1.867 \quad (3)$$

where W_a is expressed as a fraction of one. This partition was made on the basis of the relation between CI, W_a and emissivity as shown in Fig. (5). Region A for clear skies defines the area in a CI- W_a axes, where the mean value for the emissivity is lower than 0.7. Conversely, region B for completely covered skies delimits the area where emissivity is greater than 0.9. It must be emphasized that these two regions include most of the atmospheric states found, since 59 % of all the daily states are clear skies and 14 % are completely covered skies. The intermediate states correspond to partly cloudy skies or anomalies in the two previous regions, so that it is a zone with a great dispersion in the values of ϵ_a .

For “clear sky” conditions, the following expression for atmospheric emissivity ϵ_a^{cs} was derived from a polynomial fit of the available screen-level measurements in the daytime, where the non-significant terms have been discarded:

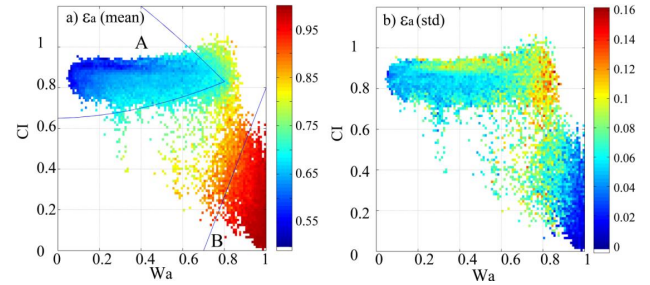


Fig. 5. (a) Mean value and (b) standard deviation for atmospheric emissivity measurements as a function of CI and W_a .

$$\epsilon_a^{cs} = -1.17 + 0.16W_a + 0.0062T_a \quad (4)$$

where W_a is expressed again as a fraction of one and T_a in K. In the case of the “completely covered skies”, the emissivity ϵ_a^{ccs} does not show any relation to T_a but it does to CI. Therefore, the following parametric function was fitted, the variables being expressed as before:

$$\epsilon_a^{ccs} = 1 - 1.38CI + 1.33W_aCI \quad (5)$$

For “partly covered skies”, the best fitted expression of the emissivity ϵ_a^{pcs} obtained was

$$\epsilon_a^{pcs} = 0.81 - 0.26CI^2 + 0.25W_a^3 \quad (6)$$

3.2.2 Local parameterization of Brutsaert, and Crawford and Duchon equations

Brutsaert (1975) analytically derived a formula to compute incident longwave radiation under clear skies assuming exponential atmospheric profiles for temperature, pressure and humidity. The theoretical background that sustains this equation has made it widely used and preferred among others. Later generalization of this equation to cloudy conditions in Brutsaert (1982) (B82) and Crawford and Duchon (1999) (CD99) added some parameterizations to this formulation. B82 extended ϵ_a^{cs} for all sky conditions by means of a factor F :

$$\epsilon_a^{cs} = lc(10e_a/T_a)^{1/7} \quad (7)$$

$$\epsilon_a = \epsilon_a^{cs} F = \epsilon_a^{cs} (1 + CN^2) \quad (8)$$

where lc stands for “leading coefficient”, originally set to 1.24, e_a is the vapour pressure near the surface in kPa, and F ($F = 1 + CN^2 \geq 1$) is the increase in the sky emissivity due to the presence of clouds. This factor is split in N , a cloud index varying between 0 for clear skies and 1 for totally overcast skies, and C , an empirical factor dependent on the cloud types, originally set to 0.22.

CD99 included two modifications to the original by B82: (1) extension to cloudy conditions through a simple linear relation between ε_a and the ratio of the measured solar irradiance to the clear-sky irradiance, s , in fact equivalent to the propagation of CI across the atmosphere; and (2) the substitution of the leading coefficient, (lc in Eq. 7) by

$$lc = (1.22 + 0.06 \sin[(\text{month} + 2)\pi/6]) \quad (9)$$

where “month” is the numerical month starting in January (=1). This expression, which results in lc values ranging from 1.28 in January to 1.22 in July, was set for Oklahoma and validated through direct measurements of atmospheric profiles. But for sites under different climate conditions, Eq. (9) should change.

It is possible to calibrate lc for a particular site using only the data of ε_a , T_a and e_a for clear sky periods in Eq. (7). At RP Station, lc was found to be constant throughout the year, with a mean value of 1.17. This is consistent with findings on the Bolivian Altiplano of Lhomme et al. (2007) ($lc = 1.18$ at 4000 m a.s.l.) and Sicart et al. (2010) ($lc = 1.15$ at 5060 m a.s.l.). This value will be used both in B82 and CD99 schemes.

As B82 uses direct measurements of cloudiness, not available at the study site, N has been parameterized using the actual screen-level values of W_a and CI in Eq. (8). This was achieved by comparing measured and simulated ε_a and the resulting parametric expression is

$$N = 1 - 0.45CI - 3.5W_aCI + 4W_a^2CI. \quad (10)$$

The value of N obtained from Eq. (10) is never allowed to be lower than 0 or higher than 1.

C in B82 also needs calibration. Data from completely covered sky periods can be used for that, so Eq. (8) has to produce $\varepsilon_a = 1$ when $N = 1$. With RP Station data, and given the previous calibration of lc , the best C was found to be 0.42.

3.2.3 Parameterization analysis

The three models proposed, 3sParam, B82, and CD99, were tested in RP Station with the calibration dataset (2004–2010 period), and with a 1-yr validation dataset (2011) which approximately represents 15 % of the whole 7-yr dataset. Furthermore, the applicability of each locally calibrated parameterization was validated with the available dataset at C Station (August 2009–April 2012) and EN2 Station (October 2009–March 2012). The goodness of agreement of each model was valued by the common statistics mean bias error (MBE), mean absolute error (MAE) and root-mean-square error (RMSE).

4 Results and discussion

Figure 6 shows the comparison between daytime ε_a measurements and values estimated by the different models for the

calibration period at RP Station. Figure 7 shows the same comparison but for the validation at C Station, the study site most different from the RP Station, using the local calibration for the RP Station. The complete results from the statistical analysis of all three models for the calibration and the three validation datasets, RP Station, C Station, and EN2 Station, are shown in Table 1. There, the results for the complete day-time data for each case along with the separation for each of the three atmospheric states (clear, totally covered and partly cloudy skies) are presented.

The results from the calibration and validation tests at RP Station agree, so that calibration is confirmed for this site. The performance of the 3sParam model stands out over the rest of models, especially for clear and completely covered skies. Partly cloudy skies are also best represented by 3sParam, even though the differences in this state are fewer. The graphical representation of these transition states in Figs. 6 and 7 shows a greater scattering, while measurements and predictions for clear and overcast states clearly fit more tightly. B82 and CD99 are very similar for clear sky predictions, as the only difference is the set of the data that is considered cloudless. Also even though CD99 exhibits an overall good performance; very similar to B82 scheme, it fails to reproduce higher values of emissivity with completely covered skies. In this atmospheric state, measurements of ε_a clearly meet at 1, while CD99 never reaches that value. The specific local parameterization of C coefficient in B82 manages to reproduce this behaviour more precisely, at the cost of the calibration of a second parameter.

The results of the validation at the lower site of C Station show an outstanding loss of performance of the 3sParam model, when compared to the results at RP Station, particularly for the lower values of emissivity for clear skies, which are vastly underestimated by this model. The transition state is drawn with much more scattering for this model (Fig. 7c). For this dataset, the leading factor fitted with RP Station data is too small and led to a general underestimation for B82 and CD99 schemes, especially in the case of the latter. Besides, CD99 is also still penalized by its incorrect simulation of highest emissivities, whose measurements are very close to unity for this site too. B82 has substantially better behaviour than the rest of schemes for every atmospheric state and exhibits an outstanding performance despite that it was calibrated for another station. One particularity of the measurements of ε_a that can be observed is that they are steadier at this lower site compared to what happened at RP Station.

Finally, the validation at EN2 Station, located very close to RP Station, displays a very similar behaviour and statistics for 3sParam scheme to that found at RP Station, even though measurements are even more unsteady here than in the RP site. However, models B82 and CD99 clearly get worse for all atmospheric states. The variable leading coefficient makes both models underestimate emissivity for clear skies, while covered skies with emissivities very close to 1 again are not captured by CD99. 3sParam is still the most efficient scheme

Table 1. Summary of the goodness of agreement for the new 3-state parameterization (3sParam), Eqs. (4) to (7), the Brutsaert equation (B82), and Crawford and Duchon (1999) (CD99), both locally calibrated, for different atmospheric states for the calibration and validation datasets. MBE: mean bias error; MAE: mean absolute error; RMSE: root-mean-square error.

Atmospheric state	3sParam MBE/MAE/RMSE	B82 MBE/MAE/RMSE	CD99 MBE/MAE/RMSE
Calibration. RP Station (Nov 2004–Dec 2010)			
Daytime – all data	0.000/0.045/0.065	0.005/0.052/0.072	−0.012/0.056/0.080
- Clear skies	0.007/0.037/0.055	0.026/0.044/0.060	0.006/0.039/0.056
- Covered skies	−0.002/0.025/0.040	−0.017/0.042/0.057	−0.075/0.080/0.097
- Partly cloudy	−0.013/0.070/0.092	−0.032/0.076/0.098	−0.043/0.080/0.109
Validation. RP Station (Jan 2011–Dec 2011)			
Daytime – all data	0.013/0.049/0.068	0.016/0.058/0.076	−0.001/0.058/0.080
- Clear skies	0.026/0.045/0.062	0.042/0.054/0.070	0.025/0.046/0.064
- Covered skies	−0.012/0.031/0.048	−0.026/0.047/0.062	−0.080/0.087/0.106
- Partly cloudy	−0.009/0.067/0.087	−0.030/0.075/0.095	−0.032/0.075/0.100
Validation. C Station (Aug 2009–Apr 2012)			
Daytime – all data	−0.062/0.071/0.084	−0.044/0.056/0.067	−0.069/0.071/0.083
- Clear skies	−0.082/0.084/0.092	−0.066/0.066/0.072	−0.078/0.078/0.086
- Covered skies	−0.014/0.027/0.038	0.005/0.026/0.040	−0.056/0.059/0.075
- Partly cloudy	−0.055/0.073/0.087	−0.036/0.055/0.070	−0.061/0.066/0.082
Validation. EN2 Station (Oct 2009–Mar 2012)			
Daytime – all data	0.008/0.043/0.055	−0.076/0.079/0.093	−0.088/0.091/0.105
- Clear skies	0.021/0.041/0.053	−0.076/0.076/0.083	−0.087/0.087/0.095
- Covered skies	−0.013/0.024/0.033	−0.038/0.049/0.063	−0.075/0.078/0.090
- Partly cloudy	−0.013/0.057/0.069	−0.097/0.104/0.123	−0.098/0.100/0.130

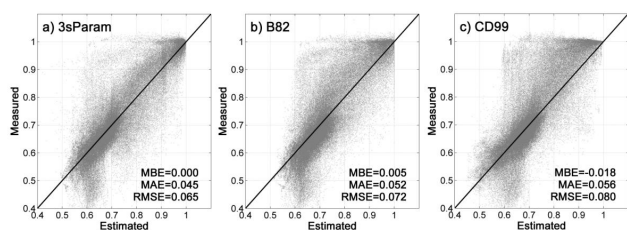


Fig. 6. Atmospheric emissivity measurements versus estimation obtained for the calibration at RP Station (2500 m a.s.l.) using the three different schemes.

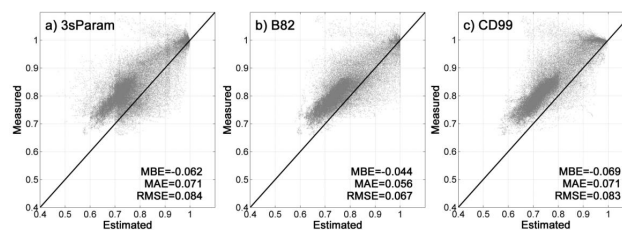


Fig. 7. Atmospheric emissivity measurements versus estimation obtained for the simulation at C Station (1332 m a.s.l.) using the three different schemes locally calibrated with RP data.

for this station, followed by B82. Since EN2 Station belongs to the same local region as RP Station, the local applicability of 3sParam can be stated, whereas a lower level of local parameterization, such as B82, can be more generally applied at the three tested sites.

The classification of the dataset in 3 atmospheric states (clear, completely covered, and partly cloudy skies) allows a better adjustment and analysis of the performance of the models. The highest error is concentrated in the intermediate atmospheric states, those with partial cloud cover, where the surface measurements are not capable of representing by themselves the complex state of the atmosphere and the presence of clouds and aerosols in it.

From Fig. 6, it can be seen that the lowest values for measured ϵ_a at RP Station, those between 0.4 and 0.5, are grouped in a scattered cloud of points with an estimated value of between 0.6 and 0.7. They are overestimated by all the models. In fact, these measurements were taken under similar atmospheric states, corresponding to sunny winter days with low wind speeds ($< 1 \text{ m s}^{-1}$), and this overestimation may be caused by the overheating of the pyrgeometer dome by solar radiation under insufficient ventilation. This effect has already been reported (e.g. Weiss, 1981), but it is normally not accounted for as the induced errors are low (Lhomme et al., 2007). However, in this work, the errors in measured longwave radiation may be important for these

specific meteorological conditions, with an absolute overestimation in measured ε_a of up to 0.2.

A C coefficient in the extended Brutsaert equation (Eq. 8) of below 0.42 would prevent the high values of ε_a , which are measured in very cloudy states, from being reached by B82 scheme. This is a much higher value than the 0.22 originally proposed by Brutsaert (1982). This reflects the fact that, in mountainous areas, the interaction of the clouds with the surface of the terrain and, therefore, their effect on ε_a is much more intense than in valley areas.

Clear sky data are well predicted in this mountainous site using the locally fitted leading coefficient of 1.17 in Eq. (7), as l_c was found to be constant throughout the year at RP Station, for which it was calibrated. Later analysis showed that the seasonality observed in Crawford and Duchon (1999) for l_c at their stations was in fact present at C and EN2 Stations, so local recalibration could have improved the results in them.

5 Conclusions

The high resolution longwave measurements recorded in a weather station at an altitude of 2500 m in a Mediterranean climate can be correctly estimated by most of the existing models and frequently used parameterizations, provided that some local calibration of their parameters can be performed. These measurements showed a very low atmospheric emissivity for longwave radiation values with clear skies (up to 0.5) and a great facility for reaching the theoretical maximum value of 1 with cloudy skies. So, despite the good behaviour of Brutsaert (1975) for clear skies with a leading coefficient of 1.17, the cloudiness effect considered in Brutsaert (1982) cannot be effectively added when cloud index N measurements are not available. The local relationships found between the screen-level values of temperature, relative humidity, and solar radiation by means of the clearness index with the emissivity under clear and cloudy skies allow one to define two kinds of parametric approaches with good results and a different applicability for estimations of the instantaneous values of the atmospheric emissivity: (1) a complete parametric expression, split into three atmospheric states parametrically regionalized (clear, completely covered and partly covered skies), with an outstanding performance at a local scale even with the unsteady measurements at high altitude mountainous sites; and (2) a local calibration of Brutsaert, and Crawford and Duchon expressions, with not such a good performance at a local scale when compared to the former, but with a more general applicability in other areas in case of Brutsaert. In particular, the proposed modification of Brutsaert (1982) by means of a parameterization of unobserved cloudiness data from the screen-level measurements of humidity and solar radiation has proven to have a good overall performance for all atmospheric states and, more importantly, a broader scope of applicability at different sites

without any further calibration. This is partly due to the flexibility gained in this scheme through the calibration of C coefficient in Eq. (8), which here was set to 0.42.

The need for downward longwave radiation measurements can be inferred from these results. When high accuracy is desired, the development of a local expression such as 3sParam is recommended if such data are available, which will allow medium- and long-term simulation of this component of the energy balance. However, the lack of direct measurements at every significant station at a study site can be satisfactorily compensated for by using weather data to locally calibrate the Brutsaert equation where longwave data are recorded, and to apply the resulting expression all over the study region, following the proposed methodology. As a direct result, it is also now possible to obtain atmospheric emissivity series at stations without any longwave direct measurements in the surroundings of Sierra Nevada. Complete parametric expressions should have, in general, a very local scope of applicability, as the validity of these fits is linked to their ability to characterize the state of the atmosphere, with regard to the local particularities in the atmospheric profiles of temperature and water vapour density and in the effect of cloudiness over emissivity, only with surface measurements of temperature, humidity, and solar radiation.

Acknowledgements. This work has been carried out within the Guadalfeo Project, funded by the Department of the Environment of the Regional Government of Andalusia, and partially funded by the Spanish Ministry of Science and Innovation (Research Project CGL2011-25632, "Snow dynamics in Mediterranean regions and its modelling at different scales. Implications for water resource management"). Meteorological data at EN2 Station is funded by the Sierra Nevada Global Change Observatory, Department of Agriculture, Fisheries and Environment of the Regional Government of Andalusia. M. J. Polo wishes to thank G. Gómez and J. A. Polo for their valuable support.

Edited by: B. Su

References

- Aguilar, C., Herrero, J., and Polo, M. J.: Topographic effects on solar radiation distribution in mountainous watersheds and their influence on reference evapotranspiration estimates at watershed scale, *Hydrol. Earth Syst. Sci.*, 14, 2479–2494, doi:10.5194/hess-14-2479-2010, 2010.
- Alados, L., Jiménez, J. I., and Castro, Y.: Thermal radiation from cloudless skies in Granada, *Theor. Appl. Climatol.*, 37, 84–89, 1986.
- Armstrong, R. L. and Brun, E. (Eds.): *Snow and Climate, Physical Processes, Surface Energy Exchange and Modeling*, Cambridge University Press, Cambridge, 2008.
- Barbaro, E., Oliveira, A. P., Soares, J., Codato, G., Ferreira, M. J., Mlakar, P., Božnar, M. Z., and Escobedo, J. F.: *Observational Characterization of the Downward Atmospheric Longwave Ra-*

- diation at the Surface in the City of São Paulo, *J. Appl. Meteorol. Clim.*, 49, 2574–2590, doi:10.1175/2010JAMC2304.1, 2010.
- Brunt, D.: Notes on radiation in the atmosphere, *Q. J. Roy. Meteorol. Soc.*, 58, 389–418, 1932.
- Brutsaert, W.: On a derivable formula for long-wave radiation from clear skies, *Water Resour. Res.*, 11, 742–744, 1975.
- Brutsaert, W.: *Evaporation into the Atmosphere*, D. Reidel Publishing Company, Dordrecht, 1982.
- Crawford, T. M. and Duchon, C. E.: An improved parameterization for estimating effective atmospheric emissivity for use in calculating daytime downwelling long-wave radiation, *J. Appl. Meteorol.*, 38, 474–480, 1999.
- Dera, J.: *Marine physics*, Elsevier, Amsterdam, 1992.
- Flerchinger, G. N., Xiao, W., Marks, D., Sauer, T. J., and Yu, Q.: Comparison of algorithms for incoming atmospheric long-wave radiation, *Water Resour. Res.*, 45, W03423, doi:10.1029/2008WR007394, 2009.
- Frigerio, E.: Radiación nocturna: campañas en Cachi, *Avances en Energías Renovables y Medio Ambiente*, Vol. 8, no. 2, Argentina, 2004.
- Gabathuler, M., Marty, C., and Hanselmann, K. W.: Parameterization of incoming longwave radiation in high-mountain environments, *Phys. Geogr.*, 22, 99–114, 2001.
- Herrero, J., Polo, M. J., Moñino, A., and Losada, M. A.: An energy balance snowmelt model in a Mediterranean site, *J. Hydrol.*, 371, 98–107, doi:10.1016/j.jhydrol.2009.03.021, 2009.
- Herrero, J., Aguilar, C., Millares, A., Moñino, A., Polo, M. J., and Losada, M. A.: Mediterranean high mountain meteorology from continuous data obtained by a permanent meteorological station at Sierra Nevada, Spain, *Geophys. Res. Abstr.*, EGU2011-12893, EGU General Assembly 2011, Vienna, Austria, 2011.
- Iziomon, M. G., Mayer, H., and Matzarakis, A.: Downward atmospheric irradiance under clear and cloudy skies: measurement and parameterization, *J. Atmos. Sol.-Terr. Phys.*, 65, 1107–1116, doi:10.1016/j.jastp.2003.07.007, 2003.
- Jordan, R. E., Andreas, E. L., and Makshtas, A. P.: Heat budget of snow-covered sea ice at North Pole 4, *J. Geophys. Res.*, 104, 7785–7806, doi:10.1029/1999JC900011, 1999.
- Kimball, B. A., Idso, S. B., and Aase, J. K.: A model for thermal radiation from partly cloudy and overcast skies, *Water Resour. Res.*, 18, 931–936, 1982.
- Kjaersgaard, J. H., Plauborg, F. L., and Hansen, S.: Comparison of models for calculating daytime long-wave irradiance using long term data set, *Agr. Forest Meteorol.*, 143, 49–63, doi:10.1016/j.agrformet.2006.11.007, 2007.
- König-Langlo, G. and Augstein, E.: Parameterization of the downward long-wave radiation at the Earth's surface in polar regions, *Meteorol. Z.*, 3, 343–347, 1994.
- Kustas, W. P., Rango, A., and Uijlenhoet, R.: A simple energy budget algorithm for the snowmelt runoff model, *Water Resour. Res.*, 30, 1515–1527, 1994.
- Lhomme, J. P., Vacher, J. J., and Rocheteau, A.: Estimating downward long-wave radiation on the Andean Altiplano, *Agr. Forest Meteorol.*, 145, 139–148, doi:10.1016/j.agrformet.2007.04.007, 2007.
- Ohmura, A.: Physical Basis for the Temperature-Based Melt-Index Model, *J. Appl. Meteorol.*, 40, 753–761, 2001.
- Philipona, R., Dürr, B., Marty, C., Ohmura, A., and Wild, M.: Radiative forcing – measured at Earth's surface – corroborate the increasing greenhouse effect, *Geophys. Res. Lett.*, 31, L03202, doi:10.1029/2003GL018765, 2004.
- Pirazzini, R., Nardino, M., Orsini, A., Calzolari, F., Georgiadis, T., and Levizzani, V.: Parameterization of the downward longwave radiation from clear and cloudy skies at Ny Ålesund (Svalbard), in: *IRS 2000: Current Problems in Atmospheric Radiation*, 559–562, A. Deepack Publishing, Hampton, Virginia, 2000.
- Plüss, C. and Ohmura, A.: Longwave radiation on snow-covered mountainous surfaces, *J. Appl. Meteorol.*, 36, 818–824, 1997.
- Prata, A. P.: A new long-wave formula for estimating downward clear-sky radiation at the surface, *Q. J. Roy. Meteorol. Soc.*, 122, 1127–1151, doi:10.1002/qj.49712253306, 1996.
- Sedlar, J. and Hock, R.: Testing longwave radiation parameterizations under clear and overcast skies at Storglaciären, Sweden, *The Cryosphere*, 3, 75–84, doi:10.5194/tc-3-75-2009, 2009.
- Sicart, J. E., Pomeroy, J. W., Essery, R.L.H., and Bewley, D.: Incoming longwave radiation to melting snow: observations, sensitivity and estimation in northern environments, *Hydrol. Process.*, 20, 3697–3708, doi:10.1002/hyp.6383, 2006.
- Sicart, J. E., Hock, R., Ribstein, P., Chazarin, J. P.: Sky long-wave radiation on tropical Andean glaciers: parameterization and sensitivity to atmospheric variables, *J. Glaciol.*, 56, 854–860, doi:10.3189/002214310794457182, 2010.
- Staiger, H. and Matzarakis, A.: Evaluation of atmospheric thermal radiation algorithms for daylight hours, *Theor. Appl. Climatol.*, 102, 227–241, 2010.
- Sugita, M. and Brutsaert, W.: Cloud Effect in the Estimation of Instantaneous Downward Longwave Radiation, *Water Resour. Res.*, 29, 599–605, doi:10.1029/92WR02352, 1993.
- Unsworth, M. H. and Monteith, J. L.: Long-wave radiation at the ground, I. Angular distribution of incoming radiation, *Q. J. Roy. Meteorol. Soc.*, 101, 13–24, doi:10.1002/qj.49710142703, 1975.
- Weiss, A.: On the performance of pyrgeometers with silicon domes, *J. Appl. Meteorol.*, 20, 962–965, 1981.
- Yang, K., He, H., Tang, W., Qin, J., and Cheng, C.: On downward shortwave and longwave radiations over high altitude regions: Observation and modeling in the Tibetan Plateau, *Agr. Forest Meteorol.*, 150, 38–46, doi:10.1016/j.agrformet.2009.08.004, 2010.